J. Eng. Technol. Sci., Vol. 54, No. 2, 2022, 220210

Isothermal Oxidation Behavior of Ferritic Oxide Dispersion Strengthened Alloy at High Temperatures

Eddy Agus Basuki [1, *], Nickolas Adrianto[1], Rahmadhani Triastomo[1], Akhmad Ardian Korda[1], Tria Laksana Achmad[1], Fadhli Muhammad[1] & Djoko Hadi Prajitno[2]

[1]Department of Metallurgical Engineering, Faculty of Mining and Petroleum Engineering, Institut Teknologi Bandung, Jalan Ganesa No. 10, Bandung 40132, Indonesia
[2]Nuclear Technology Center for Materials and Radiometry, National Atomic Agency of Indonesia, Jalan Tamansari No. 71, Bandung 40132, Indonesia
*Email: basuki@mining.itb.ac.id

Highlights:

- More detailed characterization of the mechanism of oxidation in ODS Fe-16Cr-4Al-1Ni-0.4ZrO2 alloy at 700 °C, 800 °C, and 900 °C compared with other published findings.
- The provided high temperature oxidation parabolic rate equations for three test temperatures indicated very high oxidation resistance of the alloy.
- The appearance of vacancies and voids underneath oxide scales was revealed, which play a role in the development of various oxides.

Abstract. This paper discusses the oxidation behaviors of ODS steel alloy of Fe-16Cr-4Al-1Ni-0.4ZrO_2 at 700 °C, 800 °C, and 900 °C. X-ray diffraction (XRD) as well as X-ray mapping in a scanning electron microscope were used to characterize the oxidation behavior of the samples. The rate of oxidation was measured based on the thickness of the oxide formed on the surface of the samples. Six types of oxides were identified in all ODS Fe-16Cr-4Al-1Ni-0.4ZrO_2 alloy samples after the oxidation tests, dominated by Fe_2O_3, Fe_3O_4, Cr_2FeO_4, $AlFeO_3$, Al_2FeO_4, and $AlFe_2O_4$. The oxidation kinetics of ODS Fe-16Cr-4Al-1Ni-0.4ZrO_2 steel at 700, 800, and 900 °C followed logarithmic oxidation rate behavior.

Keywords: *ferritic steel; interdiffusion; isothermal oxidation; mechanical alloying; oxide dispersion strengthening.*

1 Introduction

Nuclear power plants currently supply 11% of world energy demand, which will continue to increase in the future [1] as such power plants are do not contribute to the green-house effect. The development of nuclear power generation now has reached Generation IV, ensuring higher reliability, safety, and sustainability [2]. Higher efficiency of power generation requires higher operating temperatures,

Received December 1st, 2020, Revised May 10th, 2021, Accepted for publication July 8th, 2021.
 ISSN: 2337-5779, DOI: 10.5614/j.eng.technol.sci.2022.54.2.10

which has consequences especially for the cladding of high-pressure vessels in the reactors [3]. This part serves to protect the outer layer of the blanket wall from oxidation conditions at core outlet temperatures of up to 1,000 °C in future Very High Temperature Reactors (VHTR), much higher than in the current Light Water Reactors (LWR), which are operated at only about 400 °C [4]. Beside irradiation, the cladding material suffers from rigorous oxidation attacks at higher temperatures.

Efforts to develop ferritic chromium steel alloys used as high temperature materials for Generation IV nuclear reactors have been intensively carried out [5]. High temperature oxidation resistance of the steel is provided by a protective scale of chromia (Cr_2O_3). This oxide, however, is unstable at temperatures higher than 900 °C due to further oxidation forming volatile oxide of CrO_3 [6]. Improvement of ferritic Fe-Cr based materials by addition of aluminum to produce alumina forming ferritic steel is done to form higher stability of alumina (Al_2O_3) as a protective layer that acts together with chromium as oxygen getter [7]. Meanwhile, carbide particles acting as strengthener of the steel tend to coarsen and reduce the creep strength of the material [8]. Therefore, oxide dispersion strengthened (ODS) alloys have been developed involving nano size particles of oxides such as Y_2O_3, which have no coarsening effect [9]. Several other oxides have been considered as dispersoid strengthener in ferritic ODS steels [10], but most studies focused on microstructural evaluation and mechanical properties [11,12]. While most high temperature ferritic ODS steels involve Y_2O_3 as nano strengthener particles, only limited investigation has been done on ZrO_2 [13,14]. Recently, a study on the oxidation characteristics of ZrO_2 ODS ferritic steel with a chemical composition of Fe 25 wt.% Cr and 0.5 wt.% ZrO_2 has been done [15]. A systematic study on the oxidation behavior of alumina forming ferritic ZrO_2 ODS steels at higher temperatures still needed to be carried out. The present study aimed to determine the isothermal oxidation behavior of ferritic ODS steel alloy of Fe-16Cr-4Al-1Ni-0.4ZrO_2 at 700, 800, and 900 °C.

2 Experimental Work

ODS alloy of 78.6Fe-16Cr-4Al-1Ni-0.4ZrO_2 was prepared from high-purity raw powders of Fe (150 μm), Cr (44 μm), Al (10 μm), Ni (50 μm) and ZrO_2 (30-60 nm). The powders were mixed in a vial with 316 stainless steel balls at a powder to ball weight ratio of 10 to 1. Mechanical alloying was conducted in a planetary ball mill at 1,920 rotation per minutes for 2 h. The as-milled powders were then compacted to form green compacted ODS buttons. Sintering was carried out by heating the buttons at 1,000 °C for 6 h in total, under high-purity argon atmosphere. The as-sintered buttons were then cut into several sample coupons using a low-speed diamond cutting machine. Using an electric furnace, oxidation

tests were carried out by heating the sample coupons in air at 700, 800 and 900 °C for 5, 20, 50, and 100 h.

X-ray diffraction (XRD) was used to characterize the oxides formed on the surface of the samples using a Rigaku SmartLab X-ray diffractometer equipped with Match software. The morphologies and chemical compositions of the oxides on the oxidized samples were obtained using a scanning electron microscope (SEM) with an energy dispersive spectroscope (EDS) attached. The instrument used was a JEOL JSM-6510A analytical scanning electron microscope operated at an accelerated voltage of 15.0 kV. The kinetics of the oxidation process at different temperatures were measured based on the thickness of the oxides formed on the samples [16] by measuring at 15 different positions on the SEM image to get the average thickness of the samples.

3 Results and Discussion

Figure 1 shows the SEM micrograph and the X-ray mapping of the as-milled powders. This result showed that the mechanical alloying provided the pre-sintered raw materials for the ODS alloy. Sintering the as-milled powders at 1000 °C for 6 h resulted in an almost fully sintered alloy, as shown in Figure 2.

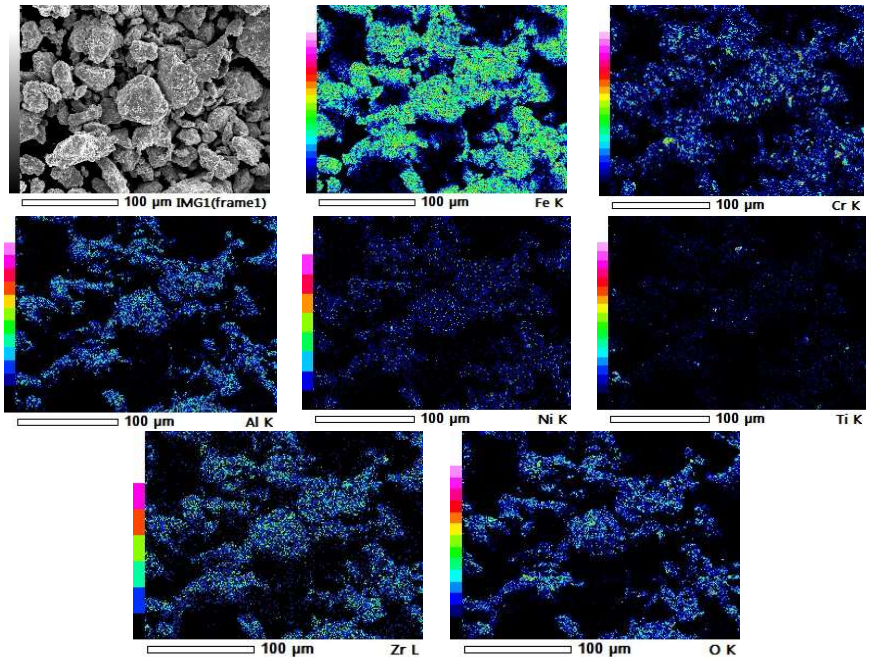

Figure 1 SEM micrograph and X-ray mapping of the as-milled alloy powder.

The X-ray mappings of all alloying elements as well as zirconia indicate a homogeneous distribution of the elements and reinforced nano particulates in the ODS alloy. The EDS analysis showed that the average chemical composition of the as-sintered ODS was 75.27% Fe, 18.32% Cr, 4.64% Al, 0.97% Ni, 0.74% Ti, and 0.05% ZrO_2.

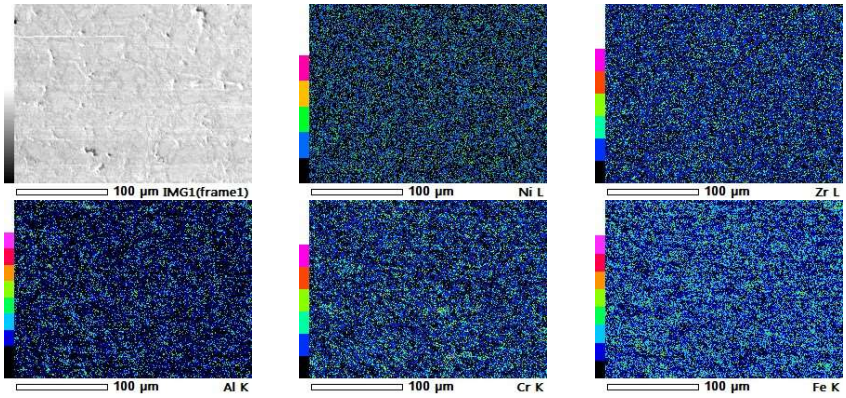

Figure 2 SEM micrograph and X-ray mapping of the as-sintered ODS alloy.

Isothermal oxidation of the alloy resulted in the formation of scales of various oxides on the surface of the ODS samples, indicated by the XRD patterns of surface scales on the samples shown in Figures 3-5. The first oxide formed was Fe_2O_3, followed by Fe_3O_4, which occurred on the Fe_2O_3-alloy interface due to lower oxygen partial pressure. Outward diffusion of Fe^{2+} and Fe^{3+} and inward diffusion of O^{2-} in Fe_3O_4 scales cause the formation of FeO. However, over longer times this iron oxide reacts with the chromia and alumina formed underneath of iron oxides, forming spinels: $Cr_2O_3 + FeO \rightarrow Cr_2FeO_4$ and $Al_2O_3 + FeO \rightarrow Al_2FeO_4$ [17]. These spinels contribute to increased oxidation resistance of the material, as found by other researchers [18]. The composition of the scales in the samples indicated that in addition to chromia spinels, oxidation at higher temperature and longer times led to the formation of alumina spinels.

Figures 6 and 7 show the morphologies of the scale oxides on the surface of the samples oxidized at 700 °C, 800 °C and 900 °C, respectively, for 5 h and 100 h. Needle-like iron oxide of Fe_2O_3 was found after oxidation at 700 °C, which changed to plate-like oxide when the temperature was increased to 800 °C. At 900 °C, however, the morphology of the iron oxide further changed to rod-like or nano-rod iron oxide [19]. Needle-like iron oxide crystals were clearly observed in surrounding pores of the ODS alloy when these defects were oxidized, as shown in Figure 8. Meanwhile, Figure 9 shows nano-rod iron oxides grew in addition to plate-like iron oxides.

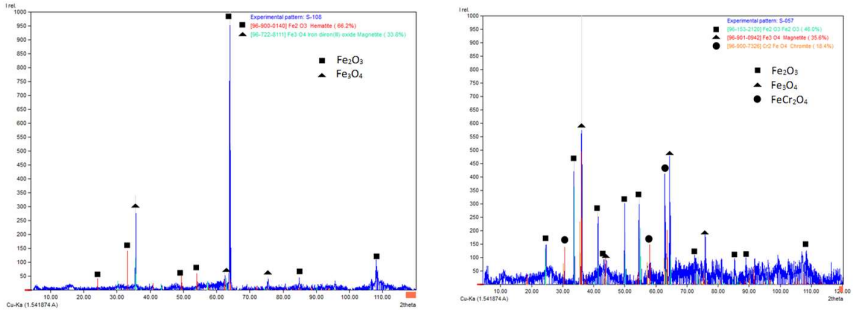

(a) (b)

Figure 3 XRD patterns of ODS alloy oxidized at 700 °C for (a) 5 h and (b) 100 h.

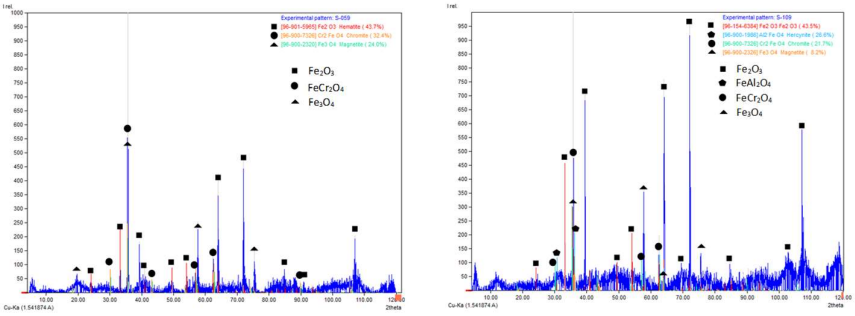

(a) (b)

Figure 4 XRD patterns of the ODS alloy samples oxidized at 800 °C for (a) 5 h and (b) 100 h.

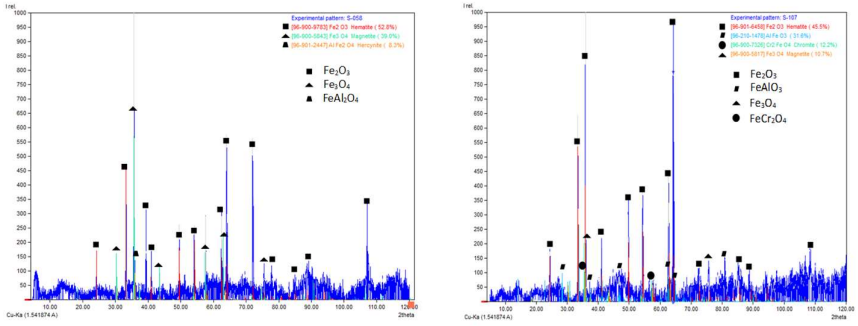

(a) (b)

Figure 5 XRD patterns of the ODS alloy samples oxidized at 900 °C for (a) 5 h and (b) 100 h.

(a) (b) (c)

Figure 6 Oxide morphologies of ODS samples oxidized for 5 h at (a) 700 ℃, (b) 800 ℃, and (c) 900 ℃.

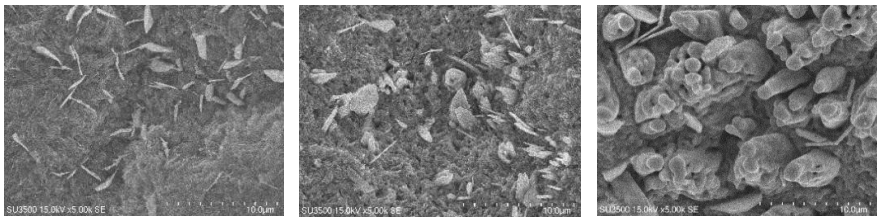

(a) (b) (c)

Figure 7 Oxide morphologies of the ODS alloy samples oxidized for 100 h at (a) 700 °C, (b) 800 °C, and (c) 900 °C.

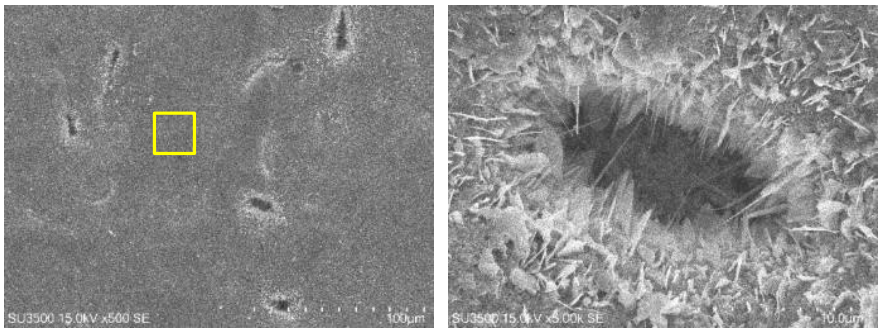

(a) (b)

Figure 8 Oxidation of pores found on some parts of the ODS alloy sample oxidized at 700 ℃ for 100 h. Microstructure of (b) is a magnification of the yellow window in (a).

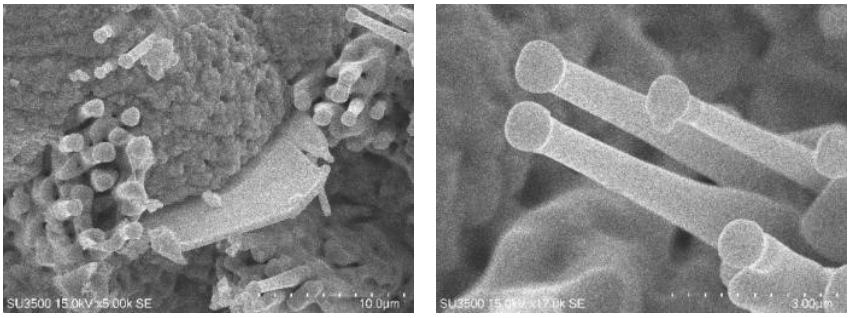

(a) (b)

Figure 9 (a) Growth of rod type and plate type iron oxides found in the ODS alloy sample oxidized at 900 ℃ for 100 h and (b) is a larger magnification of the rod-type iron oxide.

The X-ray mapping of the scale surface of the sample oxidized at 900 ℃ for 100 h, shown in Figure 10, indicates the occurrence of both spinels of Cr_2FeO_4 and $AlFeO_3$ in the outer part of the scale, supporting the finding from the XRD. However, the mass fractions of these spinels were lower compared to the iron oxides.

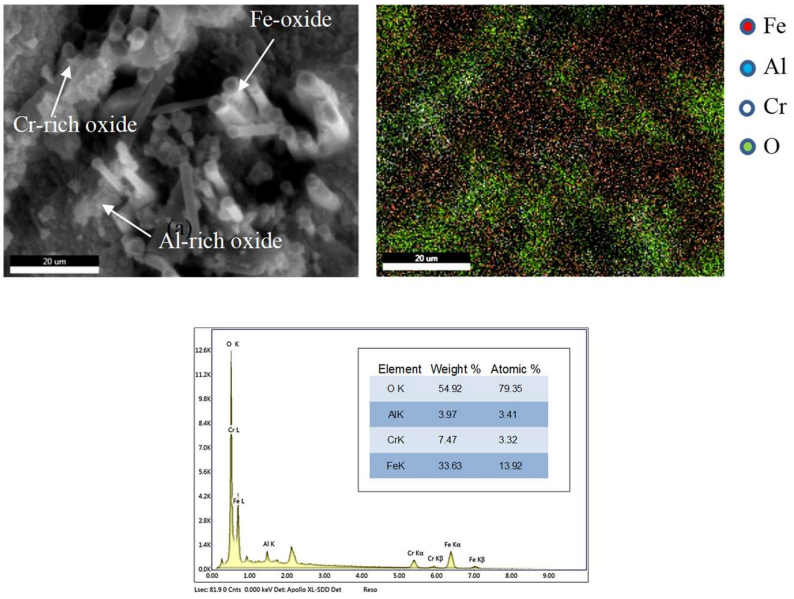

Figure 10 Surface scale morphologies during oxidation at 900 ℃ for 100 h.

Most of the spinels were obtained in lower parts of the scale. Observation of the surface of the sample oxidized at 900 °C for 100 h found an area that had experienced spalling during oxidation due to a low Pilling-Bedworth ratio (PBR) of Fe_2O_3 [8]. As depicted in Figure 11, the base part of the spalled area showed the distributions of oxide particles relatively rich in Al and Cr, indicating the positions of Cr_2FeO_4 and $AlFeO_3$ underneath the outer scale layer rich in iron oxide.

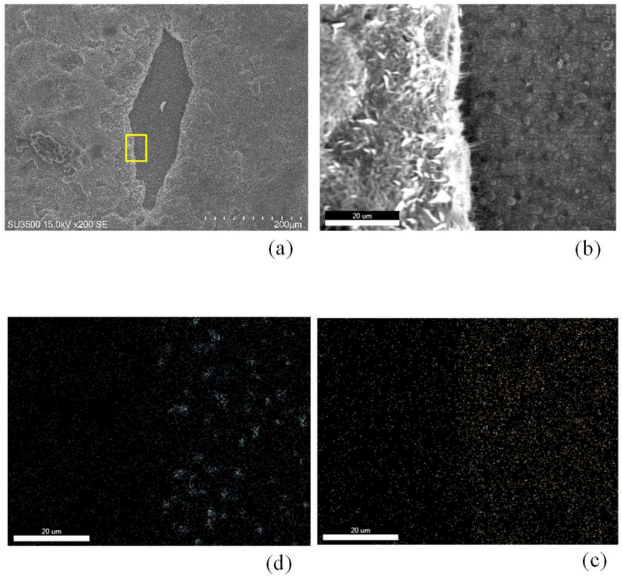

Figure 11 Identification of chromium and aluminium rich oxides in an area where the iron-oxide outer layer has spalled in the sample oxidized at 700 °C for 100 h. (a) Scanning electron micrograph of the surface experienced spalling, (b) magnification of a certain part of (a), (c) X-ray mapping of Al, and (d) X-ray mapping of Cr.

The oxidation kinetic of Fe-16Cr-4Al-1Ni-0.4ZrO_2 ODS alloy at different temperatures was measured based on the thickness of the scales on each sample for different temperatures and times. The kinetic curves are presented in Figure 12. From three possible kinetic behaviors, logarithmic behavior applies for all temperatures, i.e., x = 49.038lnt - 9.477, x = 108.89lnt - 26.472, and x = 177.96lnt – 11.142, respectively for 700 °C, 800 °C and 900 °C. Meanwhile, Figures 13 and 14 show examples of electron micrographs and the X-ray mappings of elements in the cross sections of the samples oxidized at 900 °C for 5 h and 100 h, respectively. The X-ray mappings clearly show the dominance of iron oxides in the outer scales. The EDS analysis in the area around the lower part of the scale

in the alloy oxidized at 900 °C for 100 h, shown in Figure 15, indicates the occurrence of chromium and aluminum containing oxides, expected as spinels of $FeCr_2O_4$ and $FeAl_2O_4$.

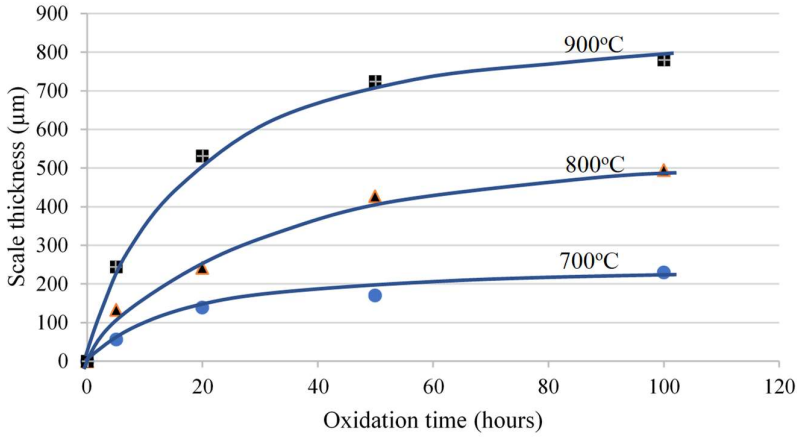

Figure 12 Oxidation kinetics of the ODS alloy samples oxidized at 700 °C, 800 °C and 900 °C.

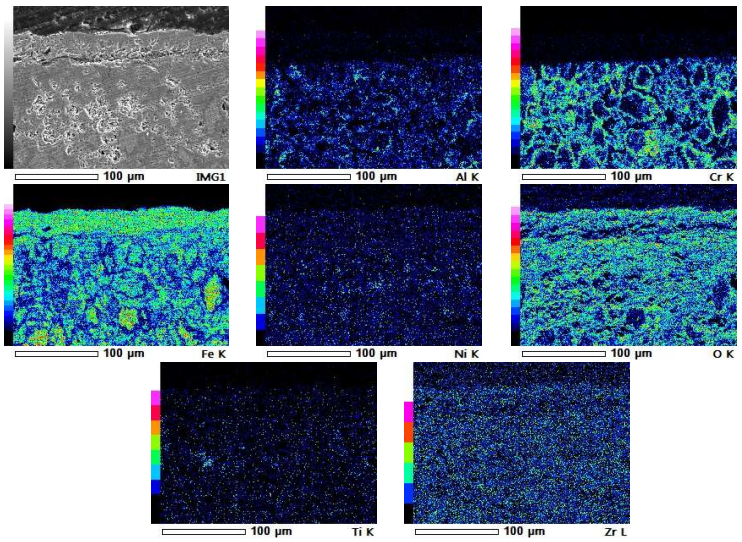

Figure 13 SEM micrograph and X-ray mapping of the ODS alloy sample oxidized at 900 °C for 5 h.

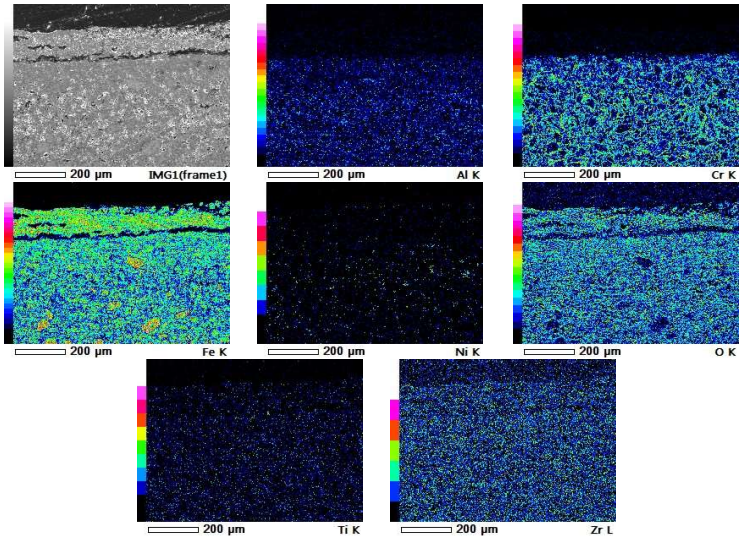

Figure 14 SEM micrograph and X-ray mapping of the ODS alloy sample oxidized at 900 °C for 100 h.

The electron micrographs of the cross section shown in Figures 13 and 14 also indicate the formation of Kirkendall voids below the iron oxides scales, often in an extended longitudinal direction parallel to the surface of the scales. Meanwhile, Figure 15 shows the interior of the void in the ODS sample oxidized at 900 ℃ for 100 h.

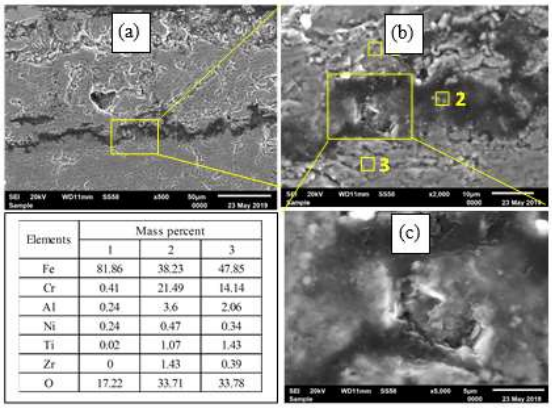

Elements	Mass percent		
	1	2	3
Fe	81.86	38.23	47.85
Cr	0.41	21.49	14.14
Al	0.24	3.6	2.06
Ni	0.24	0.47	0.34
Ti	0.02	1.07	1.43
Zr	0	1.43	0.39
O	17.22	33.71	33.78

Figure 15 EDS analysis for different locations underneath the oxide scale in the ODS alloy sample oxidized at 900 °C for 100 h.

Some particles were found attached to the walls of the voids. These particles were identified as oxides crystals of mixed oxides of ferrous as well as chromium, aluminum, as also found previously by other researchers [17]. These alumina and chromia rich oxides were expected to occur as spinels of $FeCr_2O_4$ and $FeAl_2O_4$, as also reported previously [20].

4 Conclusions

ODS steel alloy of Fe-16Cr-4Al-1Ni-0.4ZrO_2 exposed at temperatures corresponding to service overheating of 700 °C, 800 °C and 900 °C as discussed in this study gives reliable oxidation behavior, which is valuable in assessing the effect of overheating in service when ODS steel is used as cladding material in nuclear reactors. The experimental results revealed that the scales formed were dominated by iron oxides of Fe_2O_3 and Fe_3O_4. However, spinels were formed underneath the scales of $FeCr_2O_4$ and $FeAl_2O_4$. The oxidation kinetics followed logarithmic oxidation rate behavior, with the rate equations of x = 49.038lnt - 9.477, x = 108.89lnt - 26.472, x = 177.96lnt – 11.142, respectively. Coalescence of vacancies underneath the oxide scale results in voids and facilitates downward diffusion of oxygen, providing further oxidation of the ODS matrix as well as triggering scale delamination.

Acknowledment

The authors wish to acknowledge the financial support for this research work. This study was performed under the supported fund of an ITB grant through the Research, Community Services and Innovation Program (P3MI).

References

[1] International Atomic Energy Agency, *Climate Change and Nuclear Power 2018*, Vienna: International Atomic Energy Agency, 2018.

[2] Arostegui, D.A. & Holt, M., CRS Report, *Advanced Nuclear Reactors: Technology Overview and Current Issues*, Congressional Research Service, https://crsrepoerts.congress.gov, R45706, April 18, 2019.

[3] Klueh, R.L., *Oxide Dispersion Strengthened Steels: A Comparison of Some Commercial and Experimental Alloys*, Journal of Nuclear Materials, **341**, pp. 103-114, 2005.

[4] Zinkle, S.J. & Snead, L.L., *Designing Radiation Resistance in Materials for Fusion Energi*, Annual Review of Materials Research, **44**(1), pp. 241-267, 2014.

[5] Rebak, R.B., Terrani, K.A., Gassmann, W.P., Williams, J.B. & Ledford, K.L., *Improving Nuclear Power Plant Safety with FeCrAl Alloy Fuel*

Cladding, MRS Advances, **2**(21-22) (Energy and Sustainability), pp. 1217-1224, 2017.

[6] Gupta, V.K., Larsen, M. & Rebak, R.B., *Utilizing FeCrAl Oxidation Resistance Properties in Water, Air and Steam for Accident Tolerant Fuel Cladding*, ECS Trans., **85**(2), pp. 3-12, 2018. DOI: 10.1149/08502. 0003ecst.

[7] Enkvist, J., Bexell, U., Grehk, M. & Olsson, M., *High Temperature Oxidation of FeCrAl-alloys - Influence of Al-concentration on Oxide Layer Characteristics*, Materials and Corrosion, **60**(11), pp. 876-881, 2009.

[8] Birks, N. & Meier G.H., *Introduction to High Temperature Oxidation of Metals*, London, Edward Arnold, 1983.

[9] Issartel, C., Buscail, H., Chevalier, S. & Favergeon, J., *Effect of Yttrium as Alloying Element on a Model Alumina-Forming Alloy Oxidation at 1100°C*, Oxidation of Metals, **80**, pp. 409-420, 2017.

[10] Benz, H.U. & Zoz, H., *Nanostructured Ferritic Alloys (NFA) as the Next Generation ODS Manufactured by High Kinetic Processing (HKP)*, The 4th International Conference on Powder Metallurgy in Asia, Hsinchu, Taiwan, Apr. 09-11, 2017.

[11] Kumar, P.K., Sai, N.P. & Krishna, A.G., *Effect of Y_2O_3 and ZrO_2 on the Microstructure and Mechanical Properties of Nano-ODS 21Cr-9Mn-6Ni Steels*, Materials and Technology, **52**(4), pp. 493-497, 2018.

[12] Raghavendra, K., Dasgupta, A., Bhaskar, P., *et al.*, *Synthesis and Characterization of Fe-15wt.% ZrO_2 Nanocomposite Powders by Mechanical Milling*, Powder Technology, (287), pp. 190-200, 2015.

[13] Li, S., Zhou, Z., Wang, M., Hu, H., Zou, L., Zhang, G. & Zhan, L., *Microstructure and Mechanical Properties of 16Cr-ODS Ferritic Steel for Advanced Nuclear Energy System*, Journal of Physics: Conference Series **419**, 012036, 201. DOI:10.1088/1742-6596/419/1/012036.

[14] Wang, C., Luo, J., Guo, N., Tu, J., Ye, H., Zhang, P. & Yan, Q., *Effect of Yttrium Contents on the Microstructure of a Hot-Rolled Tantalum-Containing 12Cr-ODS Steel*, Frontiers in Materials, 11 December 2019, DOI: 10.3389/fmats.2019.00317.

[15] Silalahi, M, Bandriyana, B., Ahda, S., Sugeng, B. & Dimyati, A., *Synthesis and Characterization of High Chromium Zirconia Oxide Dispersion Strengthened (ODS) Steel*, IOP Conf. Series: Journal of Physics: Conf. Series **1436**, 012055, 2020. DOI:10.1088/1742-6596/1436/1/012055.

[16] Khanna, A.S., *High-Temperature Oxidation in Handbook of Environmental Degradation of Materials, Third Edition*, M. Kutz (ed.), Elsevier Inc., pp. 3-25, 2018.

[17] Narita, T. & Hayashi, S., *Internal Oxidation and Nitridation Behavior of an Fe-5 mass%Al Alloy at 1073 K*, Journal Japan Institute of Metals, **63**(10), pp. 1311-1316, 1999.

[18] Junceda, A.G., Rodriguez, N.G. & Campos, M., *Effect of Zirconium on the Microstructure and Mechanical Properties of an Al-Alloyed ODS Steel Consolidated by FAHP*, Journal American Ceramic, **11**(98), pp. 3582-3587, 2015.
[19] Chen, Z., Wang, L., Li, F. & Chou, K., *Thermodynamic Analysis of the Corrosion of Fe-16Cr Alloy Interconnect of Solid Oxide Fuel Cell under Various Atmospheres*, High Temperature Material Processing, **33**(5), pp. 439-445, 2014.
[20] Liang, T., Li, Y., Ao, R., Zhang, X. & Zeng, J., *On the Oxidation Resistance of the Compound Fe-based Protective Coating by Supersonic Arc Spraying at 1123 °K*, Proceeding of The Asia Pacific Engineering and Technology Conference, pp. 604-610, 2017.